AGU PUBLICATIONS

Geophysical Research Letters

RESEARCH LETTER
10.1002/2014GL060289

Key Points:
- Photochemical hot oxygen escape rate at Mars is predicted
- Martian exospheric neutral oxygen model is constructed
- Pickup ion fluxes measured by SEP will constrain neutral oxygen escape from Mars

Correspondence to:
T. E. Cravens,
cravens@ku.edu

Citation:
Rahmati, A., T. E. Cravens, A. F. Nagy, J. L. Fox, S. W. Bougher, R. J. Lillis, S. A. Ledvina, D. E. Larson, P. Dunn, and J. A. Croxell (2014), Pickup ion measurements by MAVEN: A diagnostic of photochemical oxygen escape from Mars, *Geophys. Res. Lett.*, *41*, 4812–4818, doi:10.1002/2014GL060289.

Received 29 MAY 2014
Accepted 2 JUL 2014
Accepted article online 3 JUL 2014
Published online 21 JUL 2014

Pickup ion measurements by MAVEN: A diagnostic of photochemical oxygen escape from Mars

A. Rahmati[1], T. E. Cravens[1], A. F. Nagy[2], J. L. Fox[3], S. W. Bougher[2], R. J. Lillis[4], S. A. Ledvina[4], D. E. Larson[4], P. Dunn[4], and J. A. Croxell[1]

[1]Department of Physics and Astronomy, University of Kansas, Lawrence, Kansas, USA, [2]Department of Atmospheric, Oceanic, and Space Sciences, University of Michigan, Ann Arbor, Michigan, USA, [3]Department of Physics, Wright State University, Dayton, Ohio, USA, [4]Space Sciences Laboratory, University of California, Berkeley, California, USA

Abstract A key process populating the oxygen exosphere at Mars is the dissociative recombination of ionospheric O_2^+, which produces fast oxygen atoms, some of which have speeds exceeding the escape speed and thus contribute to atmospheric loss. Theoretical studies of this escape process have been carried out and predictions made of the loss rate; however, directly measuring the escaping neutral oxygen is difficult but essential. This paper describes how energetic pickup ion measurements to be made near Mars by the SEP (Solar Energetic Particle) instrument on board the MAVEN (Mars Atmosphere and Volatile EvolutioN) spacecraft can be used to constrain models of photochemical oxygen escape. In certain solar wind conditions, neutral oxygen atoms in the distant Martian exosphere that are ionized and picked up by the solar wind can reach energies high enough to be detected near Mars by SEP.

1. Introduction

A wealth of evidence gathered from orbital and surface missions indicates that Mars had a much higher abundance of volatiles in its distant past [e.g., *Solomon et al.*, 2005; *Fassett and Head*, 2011] and likely had at least episodically stable liquid water [e.g., *Carr*, 1996; *Leshin et al.*, 2013]. A major goal of the NASA MAVEN (Mars Atmosphere and Volatile EvolutioN) mission is to quantify atmospheric loss processes (nasa.gov/maven), and an important loss process is the escape of neutral oxygen generated by ionospheric and thermospheric photochemistry [*Chassefière and Leblanc*, 2004]. The major neutral species in the Martian thermosphere are CO_2 and O [*Nier and McElroy*, 1977], and the major ion species is O_2^+ [*Hanson et al.*, 1977], which is created via the reaction of CO_2^+ with atomic oxygen, as well as by other ion-neutral reactions [*McElroy et al.*, 1977; *Chen et al.*, 1978; *Huestis et al.*, 2008]. The main source of the production of hot oxygen atoms in the Martian upper atmosphere is the dissociative recombination (DR) of O_2^+ in the ionosphere:

$$\begin{aligned} O_2^+ + e^- &\rightarrow O(^3P) + O(^3P) + 6.99\ \text{eV}\ (0.22) \\ &\rightarrow O(^3P) + O(^1D) + 5.02\ \text{eV}\ (0.42) \\ &\rightarrow O(^1D) + O(^1D) + 3.06\ \text{eV}\ (0.31) \\ &\rightarrow O(^1D) + O(^1S) + 0.84\ \text{eV}\ (0.05) \end{aligned} \quad (1)$$

The branching ratios given in parentheses are from *Kella et al.* [1997]. A comprehensive review on the measurements of the branching ratios for each channel of this reaction is provided by *Fox and Hać* [1997]. Half of the excess energy is carried by each atom as they go off in opposite directions in their center of mass frame. The escape energy of an O atom at 200 km is 2 eV, so that atoms created in the first two channels have speeds exceeding the escape speed and thus can potentially escape from the planet, as well as help populating a hot O exosphere.

Once produced, hot O collides with background neutral species, changing direction and losing energy. Several hot O transport models have been constructed to simulate this, including two-stream, Monte Carlo, and DSMC (Direct Simulation Monte Carlo) models [e.g., *Nagy and Cravens*, 1988; *Ip*, 1990; *Kim et al.*, 1998; *Hodges*, 2000; *Fox and Hać*, 2009, 2014; *Valeille et al.*, 2009a, 2009b, 2010a, 2010b; *Yagi et al.*, 2012; *Lee et al.*, 2013; *Gröller et al.*, 2014]. But these photochemical escape rate calculations vary by about 2 orders of magnitude as summarized in Table 3 of *Fox and Hać* [2009], and there is a lack of direct observational constraint on photochemical escape models.

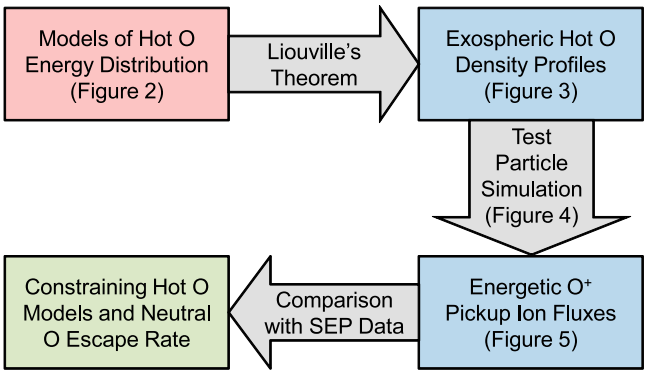

Figure 1. The methodology for constraining photochemical escape models using MAVEN SEP energetic O^+ flux measurements.

Photochemically produced hot O at Venus all remains gravitationally bound and is responsible for the oxygen corona observed via resonantly scattered solar 130.4 nm photons by the Pioneer Venus Orbiter ultraviolet spectrometer [*Nagy et al.*, 1981]. Similar measurements were made at Mars for altitudes below 1500 km by the *Rosetta* Alice far-ultraviolet imaging spectrograph [*Feldman et al.*, 2011], and similar analysis will be done using the IUVS (Imaging Ultraviolet Spectrograph) instrument on board MAVEN (lasp.colorado.edu/maven/iuvs). However, the escaping portion of the neutral oxygen exosphere at Mars is small and only dominant at distances greater than 10–15 Martian radii (R_M), as we will describe in section 2. Hence, a means of detecting distant or escaping neutral oxygen is needed in order to constrain the hot oxygen exosphere and obtain an observational check on hot O escape calculations.

The SLED (Solar Low-Energy Detector) instrument on board the Phobos 2 spacecraft made some initially puzzling measurements of energetic oxygen ions near Mars not associated with any solar or solar wind event [*McKenna-Lawlor et al.*, 1993]. *Cravens et al.* [2002] suggested that ionization of exospheric oxygen creates pickup ions far upstream of the bow shock that are sufficiently energetic near the planet (and spacecraft) to be detected by the solid-state SLED detectors. Their quantitative model-data comparisons indicated that neutral O densities of 7 cm^{-3} at about 10 R_M upstream of Mars would be consistent with SLED's O^+ flux measurements. However, the hot O model used in that paper was quite primitive and did not produce separate radial density profiles for escaping and bound oxygen atoms. In the current paper, we use a more sophisticated two-stream/Liouville model of hot O, plus a test particle model for pickup O^+ ions to demonstrate that given favorable solar wind conditions, energetic O^+ fluxes will be measurable by the SEP (Solar Energetic Particle) instrument on MAVEN and can be used to place quantitative constraints on the photochemical channel of oxygen escape from Mars. The methodology described in this study can be applied to different hot oxygen models to provide an observational test for photochemical escape estimates (Figure 1).

2. Description of the Hot Oxygen Model

The hot oxygen model to be tested in this study is constructed using a two-stream method to solve for the upward and downward hot O fluxes as a function of altitude and energy [*Nagy and Banks*, 1970; *Nagy and Cravens*, 1988; *Kim et al.*, 1998]. The ionospheric density profiles for the O_2^+ ions, electrons, and six background species (CO_2, O, N_2, CO, Ar, and O_2) are taken from a dayside radial cut of the University of Michigan's MTGCM (Mars Thermospheric General Circulation Model) for solar cycle maximum [*Bougher et al.*, 2009; *Bougher*, 2012], which are upper limit conditions that slightly exceed what MAVEN is likely to experience. The electron temperatures, which are required in determining the O_2^+ DR rate coefficients, and the ion temperatures, which are necessary for determining the nascent O speeds, are also taken from the MTGCM. These conditions were chosen to mimic data from the Viking Retarding Potential Analyzer [*Hanson et al.*, 1977; *Hanson and Mantas*, 1988].

The primary production rate of hot O is given by O_2^+ DR rate of 2α $[O_2^+]$ $[n_e]$, where $[O_2^+]$ and $[n_e]$ are the O_2^+ and electron ionospheric densities, respectively, and the total DR rate coefficient used is $\alpha = 2 \times 10^{-7}$ $(cm^3\,s^{-1})$ $(300/T_e)^{0.7}$, where T_e is the electron temperature in Kelvin. This rate coefficient approximates the range of values given in Table 1 of *Fox and Hać* [2009]. The factor of 2 in the production rate reflects the fact that two oxygen atoms are produced in the DR reaction. The nascent hot O energy distribution is taken from the Monte Carlo calculations of *Fox and Hać* [2009]. The forward and backscatter probabilities and energy losses needed in the two-stream calculation of the cascade and secondary O productions

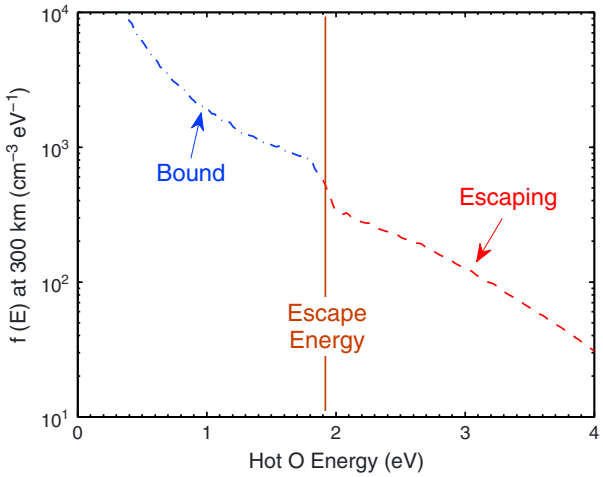

Figure 2. The two-stream calculation of hot O energy distribution function at an altitude of 300 km. The photochemical escape flux associated with this distribution is 9×10^7 cm^{-2} s^{-1}. Neutral oxygen atoms at 300 km with energies less than 1.9 eV are gravitationally bound and will not contribute to photochemical escape.

are computed by a Monte Carlo simulation of the collision of hot O with each background species. The scattering cross sections are assumed to be energy dependent and forward peaked [*Balakrishnan et al.*, 1998; *Kharchenko et al.*, 2000].

Once hot O fluxes are calculated, the hot O energy distribution function at an altitude of 300 km is found using $f(E) = (\varphi^+ + \varphi^-)/v(E)$, where φ^+ and φ^- are the upward and downward hot O fluxes, respectively, and $v(E)$ is the velocity of hot O atoms with energy E. This energy distribution function is plotted in Figure 2, and the averaged total dayside photochemical escape rate associated with this distribution is 7×10^{25} s^{-1}. Assuming that hot O atoms undergo no collisions above 300 km, exospheric densities are calculated using Liouville's theorem [*Schunk and Nagy*, 2009], where the energy distribution function is fed into a Liouville code to find the hot O number density as a function of altitude in the Martian exosphere out to 100 R_M. This is done separately for the bound and escaping portions of the distribution. As seen in Figure 3, the hot O density corresponding to the escaping part of the exospheric neutral oxygen becomes dominant at radial distances greater than 50,000 km.

3. Testing the Hot Oxygen Model

In this section we use a two-stream/Liouville model as an example of a hot O model to show that measuring the fluxes of O^+ pickup ions created via the ionization of the neutral exosphere of Mars can be used as a means of constraining the exospheric neutral oxygen density profiles predicted by hot oxygen models. We used a test particle code that tracks the trajectories of ions and computes the energy spectrum of O^+ pickup ions by recording the kinetic energy of the ions at a location (i.e., possible spacecraft location) upstream of Mars and where the solar wind is unperturbed. Oxygen ions are created in the simulation space based on the specified exospheric neutral density profile. Once O^+ ions are created, they are acted upon by the Lorentz force due to the interplanetary magnetic field, B, and the solar wind convective electric field, $E = -U_{sw} \times B$, where U_{sw} is the solar wind velocity (Figure 4). For the current paper, we adopted uniform solar wind fields of $U_{sw} = 500$ km/s and $B_y = 4$ nT, appropriate for observations made upstream of the bow shock, but this can be easily generalized. *Cravens et al.* [2002] used fields from an MHD model, appropriate for Phobos 2 solar wind conditions, and in practice solar wind conditions to be measured by MAVEN will be used.

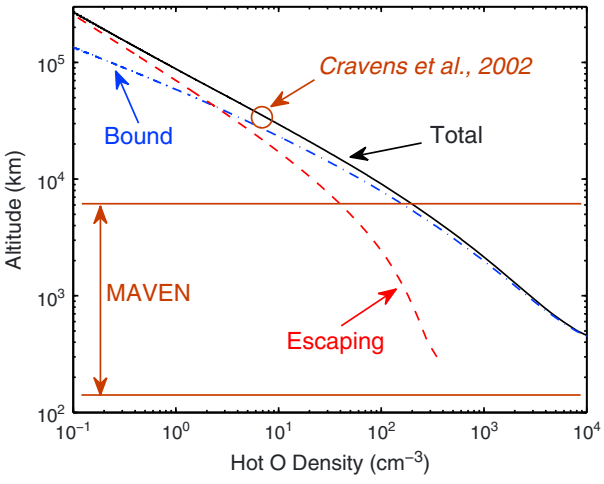

Figure 3. The density profiles of hot O in the exosphere of Mars separated for gravitationally bound and escaping neutral oxygen atoms. The escaping neutral atoms dominate the exospheric densities at distances greater than 50,000 km. The O density estimated from Phobos 2 energetic ion data [*Cravens et al.*, 2002] is shown by the circle.

Absolute O^+ fluxes are determined using the ratio of the number of simulated test particles to the actual number of ions created per second in the Martian exosphere.

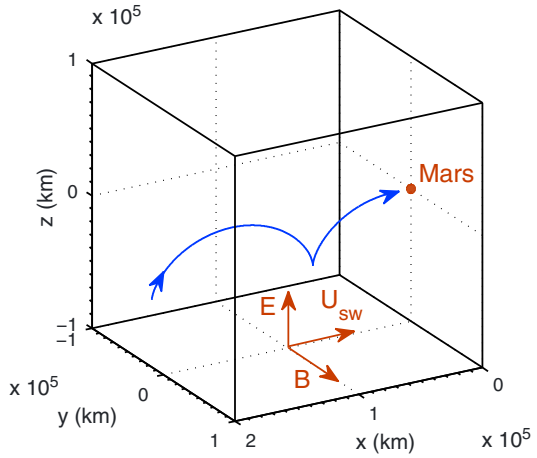

Figure 4. The trajectory of an O^+ ion calculated analytically for uniform solar wind fields. The directions of unperturbed solar wind velocity (U_{sw}), magnetic field (B), and convective electric field (E) are shown. The coordinate system is Mars centered with the x axis directed sunward, the z axis normal to the ecliptic plane, and the y axis completing the right-handed coordinate system.

The latter number is determined by multiplying the ionization frequency associated with solar radiation by the integrated exospheric density over the simulation volume, which extends far out to 100 R_M. For this paper, a constant upper limit ionization frequency of $4.5 \times 10^{-7}\,s^{-1}$ is used [*Cravens et al.*, 1987], which will be revised depending on the actual solar activity and solar wind conditions during MAVEN's science mission.

It is evident from Figure 4 that O^+ pickup ions have large gyroradii compared to the Martian radius and that the trajectories are cycloidal, as expected [*Kecskemety and Cravens*, 1993]. The gyroradius of an O^+ pickup ion in uniform solar wind fields is $r_g = m_O U_{sw} \sin(\theta_{UB})/q_O B$, where m_O and q_O are the mass and electric charge of an oxygen ion, respectively, and θ_{UB} is the angle between U_{sw} and B, which was chosen 90° for this paper, giving a gyroradius of 20,000 km. Oxygen ions travel a distance of $2\pi r_g$ downstream in one gyroperiod and will have their greatest kinetic energy when they are in the middle of one full gyroperiod. Therefore, the most energetic O^+ ions in the vicinity of Mars originate from ~20 R_M upstream, and their energy in the vicinity of Mars will be $E_{max} = 2\, m_O\, U_{sw}{}^2 \sin^2(\theta_{UB})$, giving a maximum pickup ion energy of $E_{max} = 83$ keV. The exospheric neutral oxygen at 20 R_M is mainly populated with neutral oxygen atoms that are escaping the planet. Therefore, measuring the fluxes of O^+ ions near Mars with energies close to E_{max} will provide a direct link to the escape rate of neutral oxygen atoms.

Figure 5 shows fluxes of O^+ ions as a function of their kinetic energy computed by the test particle code at an altitude of 6200 km upstream, where MAVEN's apoapsis will be located at certain times during MAVEN's science mission. The energies of pickup ions at Mars depend on how far upstream the ions are created, and the respective O^+ fluxes are proportional to hot O densities at those distances. The densities are in turn functions of the energies of hot O atoms as they leave the lower exosphere. Accordingly, determining the energy spectrum of O^+ can constrain the modeled hot oxygen energy distribution. A particular energetic particle instrument only measures part of the total ion spectrum, but in the model results, we have denoted the total O^+ fluxes and the portions associated with the bound and escaping exospheric neutral oxygen atoms. As seen in Figure 5, the predicted total O^+ fluxes between 50 keV and 83 keV are dominated by O^+ ions created in the distant exosphere, where most of the neutral oxygen atoms are not gravitationally bound and are escaping. Thus, the high-energy part of the O^+ energy spectrum is proportional to the photochemical escape rate, and measuring the flux of energetic O^+ ions in that energy range will put constraints on the modeled neutral oxygen escape rates.

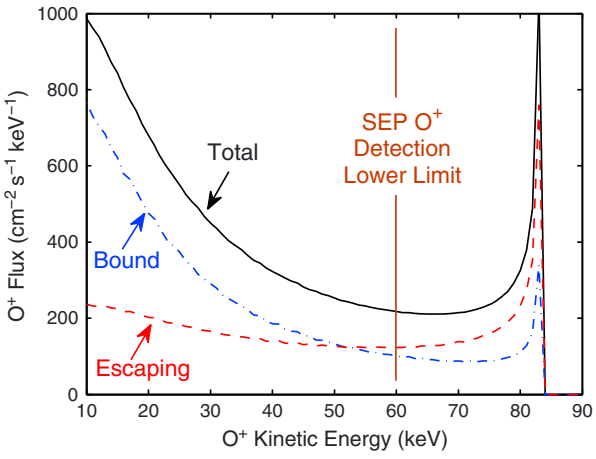

Figure 5. The energy spectrum of O^+ ions at an altitude of 6200 km upstream of Mars. High-energy parts of the O^+ flux energy spectrum and detectable by SEP (O^+ energy at 6200 km upstream >60 keV) are mainly associated with escaping hot O atoms (hot O energy at 300 km, >1.9 eV). The actual O^+ fluxes will be evaluated and compared with SEP data for different parts of the MAVEN orbit over the mission.

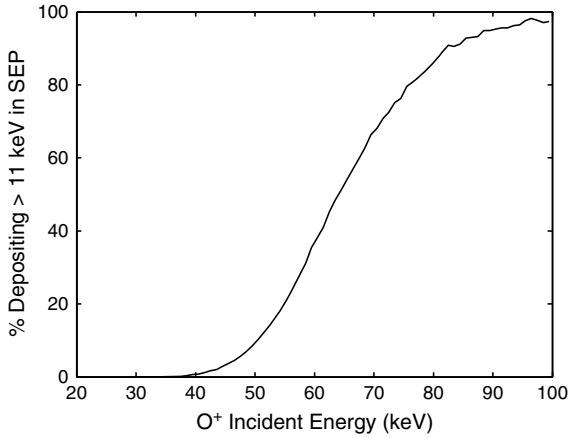

Figure 6. The fraction of oxygen ions, as a function of their incident energy that will result in at least 11 keV (SEP's electronic noise threshold) being deposited in the SEP silicon detectors past the dead layers. The curve shows the SEP oxygen detection efficiency averaged over the four detectors (SEP 1A, 1B, 2A, and 2B).

4. Discussion

The neutral oxygen escape associated with photochemically produced hot oxygen atoms via the DR reaction of O_2^+ is believed to be a major component of the total atmospheric loss from Mars [*Chassefière and Leblanc*, 2004]. Several hot O models exist and are also being developed in addition to the two-stream method that is used here to interpret the upper atmospheric data from MAVEN and determine the photochemical oxygen escape rate from Mars. Since the escaping neutral atoms are not directly measurable by MAVEN, it will be necessary to assess the output of the models and the escape rate calculations with experimental data. Energetic O^+ flux measurements to be made near Mars by the SEP instrument on board MAVEN (lasp.colorado.edu/maven/sep) can be used to determine neutral oxygen densities in the distant part of the exosphere as described in section 3. Hence, such measurements will provide observational checks on various model calculations of exospheric neutral oxygen density and photochemical escape rate.

For the parameters used in our model, an integrated O^+ flux of 4600 $cm^{-2}\,s^{-1}$ over the energy range of 70–83 keV is predicted to be measured by a Sun-pointing detector; 65% of this O^+ flux is associated with escaping neutral oxygen atoms. Of course, the SEP instrumental geometry, response function, field of view, and look directions will need to be included in an actual analysis, just as *Cravens et al.* [2002] did for SLED on the Phobos 2 mission. Simulations of SEP oxygen detection efficiency indicate that on average, O^+ ions with kinetic energies greater than 60 keV will deposit enough energy in SEP's silicon detector to be detectable (Figure 6). Therefore, the necessary observations by SEP are possible given the presence of appropriate solar wind conditions and the absence of solar particle events. For an O^+ pickup ion to have a maximum energy of $E_{max} > 60$ keV to be detected by SEP, solar wind speeds of 500 km/s or higher, with θ_{UB} exceeding ~50°, are needed, and statistically, such conditions occur ~20% of the time [*Rangarajan and Barreto*, 2000; *Jarvinen and Kallio*, 2014]. During intense solar particle events, the flux of solar energetic particles associated with solar flares and coronal mass ejections will likely exceed the predicted pickup ion fluxes. However, on average, these solar events only occur a few times a month [*Reames*, 2004; *Jun et al.*, 2007].

Test particle simulations of ion transport and escape associated with the ionization of the neutral corona at radial distances below ~5 R_M [e.g., *Fang et al.*, 2008; *Curry et al.*, 2013] can be compared with the measurements of the STATIC (Suprathermal and Thermal Ion Composition) and SWIA (Solar Wind Ion Analyzer) instruments on board MAVEN to help the IUVS instrument in constraining the low-altitude hot O density profile. The STATIC (lasp.colorado.edu/maven/static) and SWIA instruments [*Halekas et al.*, 2013] will sample pickup ions with energies below ~30 keV, which are mostly associated with the low-altitude and bound neutral oxygen corona. However, the escaping portion of the exospheric neutral oxygen is only dominant in the distant exosphere (above ~10 R_M), and the energetic O^+ pickup ion spectrum measured by SEP is needed to constrain the models of photochemical oxygen escape.

Acknowledgments
For information on data availability, please contact the corresponding author. This project has been supported at the University of Kansas and the University of Michigan by subcontracts from the University of Colorado LASP MAVEN grant NNH10CC04C from the NASA.

The Editor thanks two anonymous reviewers for their assistance in evaluating this paper.

References

Balakrishnan, N., V. Kharchenko, and A. Dalgarno (1998), Slowing of energetic O(^{3}P) atoms in collisions with N_2, *J. Geophys. Res.*, *103*(A10), 23,393–23,398, doi:10.1029/98JA02198.

Bougher, S. W. (2012), Coupled MGCM-MTGCM Mars Thermosphere Simulations and Resulting Data Products in Support of the MAVEN Mission, JPL/CDP report, pp. 1–9, 6 Aug.

Bougher, S. W., A. Valeille, M. R. Combi, and V. Tenishev (2009), Solar cycle and seasonal variability of the martian thermosphere-ionosphere and associated impacts upon atmospheric escape, *SAE Int. J. Aerosp.*, *4*(1), 227–237, doi:10.4271/2009-01-2396.

Carr, M. H. (1996), *Water on Mars*, Oxford Univ. Press, New York.
Chassefière, E., and F. Leblanc (2004), Mars atmospheric escape and evolution: Interaction with the solar wind, *Planet. Space Sci.*, *52*(11), 1039–1058, doi:10.1016/j.pss.2004.07.002.
Chen, R. H., T. E. Cravens, and A. F. Nagy (1978), The Martian ionosphere in light of the Viking observations, *J. Geophys. Res.*, *83*(A8), 3871–3876, doi:10.1029/JA083iA08p03871.
Cravens, T. E., J. U. Kozyra, A. F. Nagy, T. I. Gombosi, and M. Kurtz (1987), Electron impact ionization in the vicinity of comets, *J. Geophys. Res.*, *92*(A7), 7341–7353, doi:10.1029/JA092iA07p07341.
Cravens, T. E., A. Hoppe, S. A. Ledvina, and S. McKenna-Lawlor (2002), Pickup ions near Mars associated with escaping oxygen atoms, *J. Geophys. Res.*, *107*(A8), 1170, doi:10.1029/2001JA000125.
Curry, S. M., M. Liemohn, X. Fang, D. Brain, and Y. Ma (2013), Simulated kinetic effects of the corona and solar cycle on high altitude ion transport at Mars, *J. Geophys. Res. Space Physics*, *118*, 3700–3711, doi:10.1002/jgra.50358.
Fang, X., M. W. Liemohn, A. F. Nagy, Y. Ma, D. L. De Zeeuw, J. U. Kozyra, and T. H. Zurbuchen (2008), Pickup oxygen ion velocity space and spatial distribution around Mars, *J. Geophys. Res.*, *113*, A02210, doi:10.1029/2007JA012736.
Fassett, C. I., and J. W. Head (2011), Sequence and timing of conditions on early Mars, *Icarus*, *211*, 1204–1214, doi:10.1016/j.icarus.2010.11.014.
Feldman, P. D., et al. (2011), *Rosetta*-Alice observations of exospheric hydrogen and oxygen on Mars, *Icarus*, *214*, 394–399, doi:10.1016/j.icarus.2011.06.013.
Fox, J. L., and A. Hać (1997), Spectrum of hot O at the exobases of the terrestrial planets, *J. Geophys. Res.*, *102*(A11), 24,005–24,011, doi:10.1029/97JA02089.
Fox, J. L., and A. B. Hać (2009), Photochemical escape of oxygen from Mars: A comparison of the exobase approximation to a Monte Carlo method, *Icarus*, *204*, 527–544, doi:10.1016/j.icarus.2009.07.005.
Fox, J. L., and A. B. Hać (2014), The escape of O from Mars: Sensitivity to the elastic cross sections, *Icarus*, *228*, 375–385, doi:10.1016/j.icarus.2013.10.014.
Gröller, H., H. Lichtenegger, H. Lammer, and V. I. Shematovich (2014), Hot oxygen and carbon escape from the martian atmosphere, *Planet. Space Sci.*, *98*, 93–105, doi:10.1016/j.pss.2014.01.007.
Halekas, J. S., E. R. Taylor, G. Dalton, G. Johnson, D. W. Curtis, J. P. McFadden, D. L. Mitchell, R. P. Lin, and B. M. Jakosky (2013), The Solar Wind Ion Analyzer for MAVEN, *Space Sci. Rev.*, doi:10.1007/s11214-013-0029-z.
Hanson, W. B., and G. P. Mantas (1988), Viking electron temperature measurements: Evidence for a magnetic field in the Martian ionosphere, *J. Geophys. Res.*, *93*(A7), 7538–7544, doi:10.1029/JA093iA07p07538.
Hanson, W. B., S. Sanatani, and D. R. Zuccaro (1977), The Martian ionosphere as observed by the Viking retarding potential analyzers, *J. Geophys. Res.*, *82*(28), 4351–4363, doi:10.1029/JS082i028p04351.
Hodges, R. R. (2000), Distributions of hot oxygen for Venus and Mars, *J. Geophys. Res.*, *105*(E3), 6971–6981, doi:10.1029/1999JE001138.
Huestis, D. L., S. W. Bougher, J. L. Fox, M. Galand, R. E. Johnson, J. I. Moses, and J. C. Pickering (2008), Cross sections and reaction rates for comparative planetary aeronomy, *Space Sci. Rev.*, *139*, 63–105, doi:10.1007/s11214-008-9383-7.
Ip, W.-H. (1990), The fast atomic oxygen corona extent of Mars, *Geophys. Res. Lett.*, *17*(13), 2289–2292, doi:10.1029/GL017i013p02289.
Jarvinen, R., and E. Kallio (2014), Energization of planetary pickup ions in the solar system, *J. Geophys. Res. Planets*, *119*, 219–236, doi:10.1002/2013JE004534.
Jun, I., R. T. Swimm, A. Ruzmaikin, J. Feynman, A. J. Tylka, and W. F. Dietrich (2007), Statistics of solar energetic particle events: Fluences, durations, and time intervals, *Adv. Space Res.*, *40*, 304–312, doi:10.1016/j.asr.2006.12.019.
Kecskemety, K., and T. E. Cravens (1993), Pick-up ions at Pluto, *Geophys. Res. Lett.*, *20*(7), 543–546, doi:10.1029/93GL00487.
Kella, D., L. Vejby-Christensen, P. J. Johnson, H. B. Pedersen, and L. H. Andersen (1997), The source of green light emission determined from a heavy-ion storage ring experiment, *Science*, *276*, 1530–1533, doi:10.1126/science.276.5318.1530.
Kharchenko, V., A. Dalgarno, B. Zygelman, and J.-H. Yee (2000), Energy transfer in collisions of oxygen atoms in the terrestrial atmosphere, *J. Geophys. Res.*, *105*(A11), 24,899–24,906, doi:10.1029/2000JA000085.
Kim, J., A. F. Nagy, J. L. Fox, and T. E. Cravens (1998), Solar cycle variability of hot oxygen atoms at Mars, *J. Geophys. Res.*, *103*(A12), 29,339–29,342, doi:10.1029/98JA02727.
Lee, Y., M. R. Combi, V. Tenishev, and S. W. Bougher (2013), Hot oxygen corona in Mars' upper thermosphere and exosphere: A comparison of results using the MGITM and MTGCM, AGU Fall Meeting Abstracts, P21A-1703.
Leshin, L. A., et al. (2013), Volatile, isotope, and organic analysis of martian fines with the Mars Curiosity rover, *Science*, *341*(6153), doi:10.1126/science.1238937.
McElroy, M. B., T. Y. Kong, and Y. L. Yung (1977), Photochemistry and evolution of Mars' atmosphere: A Viking perspective, *J. Geophys. Res.*, *82*(28), 4379–4388, doi:10.1029/JS082i028p04379.
McKenna-Lawlor, S. M. P., V. Afonin, Y. Yeroshenko, E. Keppler, E. Kirsch, and K. Schwingenschuh (1993), First identification in energetic particles of characteristic plasma boundaries at Mars and an account of various energetic particle populations close to the planet, *Planet. Space Sci.*, *41*(5), 373–380, doi:10.1016/0032-0633(93)90071-9.
Nagy, A. F., and P. M. Banks (1970), Photoelectron fluxes in the ionosphere, *J. Geophys. Res.*, *75*(31), 6260–6270, doi:10.1029/JA075i031p06260.
Nagy, A. F., and T. E. Cravens (1988), Hot oxygen atoms in the upper atmospheres of Venus and Mars, *Geophys. Res. Lett.*, *15*(5), 433–435, doi:10.1029/GL015i005p00433.
Nagy, A. F., T. E. Cravens, J. H. Yee, and A. I. F. Stewart (1981), Hot oxygen atoms in the upper atmosphere of Venus, *Geophys. Res. Lett.*, *8*(6), 629–632, doi:10.1029/GL008i006p00629.
Nier, A. O., and M. B. McElroy (1977), Composition and structure of Mars' upper atmosphere: Results from the neutral mass spectrometers on Viking 1 and 2, *J. Geophys. Res.*, *82*(28), 4341–4349, doi:10.1029/JS082i028p04341.
Rangarajan, G. K., and L. M. Barreto (2000), Long term variability in solar wind velocity and IMF intensity and the relationship between solar wind parameters and geomagnetic activity, *Earth Planets Space*, *52*, 121–132.
Reames, D. V. (2004), Solar energetic particle variations, *Adv. Space Res.*, *34*(2), 381–390, doi:10.1016/j.asr.2003.02.046.
Schunk, R. W., and A. F. Nagy (2009), *Ionospheres: Physics, Plasma Physics, and Chemistry*, Cambridge Univ. Press, Cambridge.
Solomon, S. C., et al. (2005), New perspectives on ancient Mars, *Science*, *307*, 1214–1220, doi:10.1126/science.1101812.
Valeille, A., V. Tenishev, S. W. Bougher, M. R. Combi, and A. F. Nagy (2009a), Three-dimensional study of Mars upper thermosphere/ionosphere and hot oxygen corona: 1. General description and results at equinox for solar low conditions, *J. Geophys. Res.*, *114*, E11005, doi:10.1029/2009JE003388.
Valeille, A., M. R. Combi, S. W. Bougher, V. Tenishev, and A. F. Nagy (2009b), Three-dimensional study of Mars upper thermosphere/ionosphere and hot oxygen corona: 2. Solar cycle, seasonal variations and evolution over history, *J. Geophys. Res.*, *114*, E11006, doi:10.1029/2009JE003389.

Valeille, A., M. R. Combi, V. Tenishev, S. W. Bougher, and A. F. Nagy (2010a), A study of suprathermal oxygen atoms in Mars upper thermosphere and exosphere over the range of limiting conditions, *Icarus*, *206*(1), 18–27, doi:10.1016/j.icarus.2008.08.018.

Valeille, A., S. W. Bougher, V. Tenishev, M. R. Combi, and A. F. Nagy (2010b), Water loss and evolution of the upper atmosphere and exosphere over Martian history, *Icarus*, *206*(1), 28–39, doi:10.1016/j.icarus.2009.04.036.

Yagi, M., F. Leblanc, J. Y. Chaufray, F. Gonzalez-Galindo, S. Hess, and R. Modolo (2012), Mars exospheric thermal and non-thermal components: Seasonal and local variations, *Icarus*, *221*(2), 682–693, doi:10.1016/j.icarus.2012.07.022.